Role of side chains in phase equilibria of disklike mesogens

Maciej Wnek and Jozef K. Moscicki*
Institute of Physics, Jagiellonian University, 30-059 Krakow, Reymonta 4, Poland
(Received 5 December 1997)

A theory of phase equlibria in solutions of discotic mesogens of a hard-core disklike center and attached side chains is developed in the Flory lattice approximation. The role of the side chain stiffness and length in the phase equilibria is studied numerically in detail for two cases of the hard-core size, $x=7$ and 10. It is found that the chain stiffness has a profound effect on the molecular ordering, with stiff chains increasing and soft chains decreasing the nematic order parameter S. The critical solute concentration for the first appearance of the stable nematic phase v_x^* shifts towards lower values for stiff chains and to higher values for flexible ones. In addition, the soft chains suppress while the rigid ones enhance the coexistence range of two nematic phases observed for $x \simeq 9.1$ [M. Wnek and J. K. Moscicki, Phys. Rev. E **53**, 1666 (1996)]. [S1063-651X(98)04909-5]

PACS number(s): 61.30.Cz, 64.70.Md

I. INTRODUCTION

In the field of approximating the spatial configurations and interactions of molecules in liquids one of the most commonly used approaches is the hard-particle model. This is due to the thoroughly accepted assumption that the main contribution to the intermolecular potential is the short-range repulsive forces (steric interactions) rather than the long-range attractive forces. Other interactions, e.g., dispersion forces, are usually introduced as a perturbation. One of the very efficient methods of studying configurational order of hard particles is the Flory lattice approach developed over the years by Flory and his followers [1–7]. The theory succeeded especially in describing the isotropic to nematic phase transitions in liquids of highly asymmetric rigid and semirigid molecules in thermotropic and lyotropic systems. The great advantage of the method is the absence of low-density expansions as in Onsager models [8,9].

The formation of the nematic phase by disklike molecules was envisioned and discovered by Chandrasekhar, Sadashiya, and Sureah over twenty years ago, and since then discotic mesogens have attracted increased attention [10]. The liquid crystallinity of disklike molecules is known to be thermotropic and lyotropic in nature, and the usual nematic phase and a large variety of columnar phases are formed, the latter corresponding to the smectic order in systems of rodlike molecules [11–13]. The anisotropy of the disklike mesogen unit can vary considerably from relatively simple to large sheetlike rectangular structures [14–17]. At the forefront of current research are discotic metalomesogens because of their unique conductive and magnetic properties [18,19].

In a previous paper, we proposed a lattice method based theory of phase equlibria in a solution of disklike particles [7]. Disorder in disk orientation is limited in a dense system by the requirement that an overlap of molecules be avoided. In order to quantify the implications of this requirement for the steric part of the partition function we followed the crucial idea of Flory to represent a molecule at a given inclination to the director by a suitable number of perfectly ordered subparticles (segments); cf. Fig. 1. We considered a solution consisting of n_s isodiametric spherical solvent molecules and n_x rigid disklike molecules of the same thickness and x times as wide. The volume occupied by the solution is subdivided into a cubic array of n_0 cells of linear dimension equal to the diameter of the solvent particle (and the disk thickness). We assumed that each solvent molecule occupies fully a cell of the lattice. Similarly, each disk consisted of contiguous fully occupied cells. No voids (empty cells) were allowed in the system, thus $n_0 = n_s + x^2 n_x$.

If the nematic director is along the lattice **Z** axis, then due to the cylindrical symmetry of disklike molecules and the axial symmetry of the nematic phase, the perfectly ordered disk is approximated on the lattice by a rectangular parallelepiped of breath-to-width ratio x located in an elementary **XY** slice of the lattice; cf. Fig. 1 of [7]. Disorientation of a disk is then described via two independent rotations about **X** and **Y**, producing segmentation of the parallelepiped into a stairway structure of segments located in neighboring el-

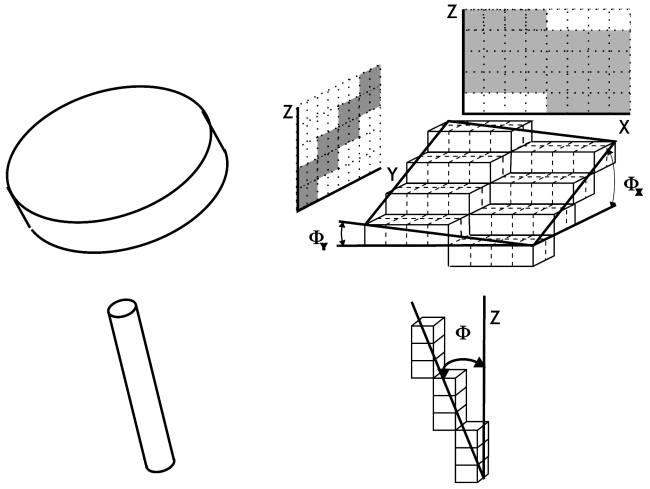

FIG. 1. Typical hard-core potentials for model disks and rods and their lattice representations. The disorder of particles is described by the ϕ angle for rods and by a pair (ϕ_x, ϕ_y) for disks; see the text.

*Electronic address: ufmoscic@cyf-kr.edu.pl

ementary **XY** slices; cf. Fig. 1. The overall disorder of the disk y is defined by the arithmetic mean of two disorder indices, y_X and y_Y referring to both declinations

$$y=(y_X+y_Y)/2. \tag{1}$$

In the spirit of the Flory method, we considered trains of contiguous segments in neighboring slices as independent from each other and their distribution in any given **XY** slice random, being uninfluenced by circumstances in neighboring slices. Furthermore, due to the positional disorder of the nematic phase, the composition of each slice should be the same. Thus the model is independent of the shape of the system volume.

The combinatorics of putting particles into the lattice incorporated their disklike nature and were quite easily solvable. The configurational part of the partition function Z_{comb} for placing n_x identical disks is

$$Z_{comb}=(n_x!)^{-1}\prod_{j+1=1}^{n_x}\nu_{j+1}, \tag{2}$$

with ν_{j+1} being the number of configurations available for the $j+1$ disk, provided j disks are already positioned on the lattice. We estimated ν_{j+1} for a disk characterized by its y_X, y_Y indices and represented on the lattice by y_X+y_Y-1 trains of contiguous subparticles to be (cf. Figs. 4 and 5 of [7])

$$\nu_{j+1}=n_0 P_1^{(y_X+y_Y-1)} P_2^{(y_X y_Y-y_X-y_Y+1)}, \tag{3}$$

where subparticles are divided into two categories depending on the conditional probability of finding room for the given subparticle in the elementary **XY** slice; the probability of finding the space for the *first* segment of each train (y_X+y_Y-1 of them) is P_1 and for every *other* it is P_2. P_1 and P_2 are in turn expressed via the conditional probabilities of finding vacant sites for all constituent cells of each category of subparticles (cf. Fig. 5 of [7])

$$P_1=p_{1a}p_{1b}^{(x/y_X+x/y_Y-2)}p_{1c}^{(x/y_X-1)(x/y_Y-1)}, \tag{4}$$

$$P_2=p_{2a}p_{2b}^{(x/y_X+x/y_Y-2)}p_{1c}^{(x/y_X-1)(x/y_Y-1)}. \tag{5}$$

Except for the first cell of each train ($1a$), probabilities p_i ($i=2a$ and $1c$) are given by the mole fraction of vacant sites in a random distribution of subparticles and empty sites

$$p_i\simeq\frac{n_0-jx^2}{n_0-j[x^2-K_i(x,\overline{y})]}, \tag{6}$$

$K_i(x,\overline{y})$ being the average disk occupation factors, the estimation of which are crucial for the theory [7]. With Z_{comb} known, as well as the usual orientational and interaction parts of the partition function, the Gibbs free energy G and thus equlibria conditions were established; cf. [7].

Numerical calculations yielded the minimum value of the disk anisotropy sufficient for the formation of the nematic phase, $x_{min}=3.015$. The result is in very good agreement with the anisotropy measured for discotic micelles in aqueous solutions [13,15,20–22]. We thoroughly discussed changes in the concentration-temperature phase diagrams resulting from the van Laar–type solute-solvent interactions as well as via disk anisotropy. The results showed a striking similarity to the phase equlibria properties of solutions of rodlike molecules with the same molecular volume as disks, in excellent agreement with results of extensive Monte Carlo simulations and results from Onsager-type models [9,23]. The phase diagrams for disks and rods of the same molecular volume were almost identical and displayed all relevant features such as triple points, nematic-nematic coexistence regions, and critical concentrations [7].

However, there is one characteristic feature for all discotic thermotropic mesogens that is often ignored in the first approximation of theoretical modeling, i.e., the presence of a number of side chains laterally attached to the hard quasidiscotic core. These side chains are usually of the alkyl type [24]. The influence of side chains on phase transitions via their length, conformation, and stiffness was observed in many experiments [25–30]. The most recent studies of large sheetlike complexes of palladium organyls in nonpolar solvents showed that, depending on the chain length and its orientation with respect to the core, different phase diagrams and different degrees of orientational order can be obtained [31,32]. What is even more striking is that two nematic phases with different degrees of order were found in this type of solution. The importance of the chain ''stiffness'' in the formation of the nematic order and in phase equlibria is emphasized by recent experimental results of Praefcke [33], which suggest that the chains preserve conformational structure to some extent and thus change the steric parameters of the system. This becomes especially important when the temperature is varied since conformational changes in the side chains influence their stiffness. The experimental data are not yet sufficiently rich for drawing any quantitative conclusions, but they definitely emphasize the importance of the chains in the formation of mesophases and phase equilibria in solutions of discotic complexes.

We therefore found it important to extend our simple theory to a more realistic system of disks with side chains. In the lattice approach we are not constrained by mean field virial expansions and ''excluded volume'' approximations that strongly depend on the molecular cylindrical symmetry (cigars or disks) and, in the case of side chains, are impossible to calculate. The lattice method is the only one that allows one to account for steric effects from side chains in the molecular configurational partition function, as well as for conformational changes in the chains. Other models, e.g., those of Onsager [34] or Gay and Berne [35], are limited to the platelike symmetry of the shape of the molecular potential and thus incorporation of the chains is almost impossible.

For rodlike molecules, the influence of molecular flexibility on the phase equlibria was considered in terms of the lattice method by Matheson and Flory [36] and for rods with fully flexible side chains by Ballauff [37]. Their important finding is that the presence of flexible side chains causes a decrease of the system order, i.e., fully flexible chains act more or less as a virtual solvent weakening the steric interactions between the anisotropic cores.

It is well established experimentally that side chain aliphatic chains are undergoing continuous conformational changes and their structure and the mean shape persistence

depend on the symmetry of environement. The isotropic environment favors more randomized conformers, while the anisotropic one supports elongated structures [39–43]. To simplify the problem, we study here two extreme cases of side chains attached in plane to the hard core, i.e., *stiff* rodlike and *soft* fully flexible ones. We assume for simplicity that all side chains are identical and preserve their flexibility/stiffness in all coexisting phases. Considering the soft side chains, we follow the approach of Matheson and Flory [36] and Ballauff [37] for rods with soft side chains, whereas the stiff chains are basically treated in a way similar to rodlike molecules [1,2].

The details of the phase diagrams obtained do not differ dramatically from the ones for pure disks [7]. However, the disordering effect of the flexible chains results in a shift of the nematic-isotropic (N-I) coexistence range towards higher concentrations and a decrease in the nematic order parameter S. The changes are roughly proportional to the chains volume fraction of the whole molecule. The N-I coexistence region, observed for bare disks of $x \geqslant 9$ (cf. [7]), becomes smaller and for sufficiently long chains disappears.

The opposite effects are observed for stiff chains. The shift of the N-I range is towards lower concentrations and the range extent is strongly enhanced. For stiff chains we also observe a proportionality between the changes in the phase diagram and the chain's length. The changes in S are not so uniform, but are similar to those obtained in [7] for pure disks on increasing their anisotropy x. So we conclude that the stiff chains effectively increase the order in the model solution. Finally, we also give some general ideas on how to incorporate more complicated chain structures such as chains attached at a certain angle to the hard core or chains that are partially stiff and partially flexible.

II. THEORY

The theory presented here is a generalization of [7] to a system of molecules (referred to hereafter as discotics or solute molecules) with disklike hard cores (bare disks) and laterally attached identical side chains. In calculating the number of ways the solute molecules can be placed into a limited volume, the theory follows closely from our previous work. What is significantly different is that side chains are now attached at the parallelepiped corners that (i) require additional empty cells on the lattice and (ii) themselves cause additional packing restrictions.

The partition function of an assembly of the molecules Z is usually factorized, i.e.,

$$Z = Z_{comb} Z_{or} Z_{int}, \tag{7}$$

where the three factors are the combinatoric or steric factor Z_{comb}, the orientational factor Z_{or}, and the factor introducing the exchange free energies of interaction between the molecules Z_{int}. A perfectly ordered hard core of volume x^2 is approximated as before by an $x \times x \times 1$ rectangular parallelepiped with its long edges parallel to the **X** and **Y** axes of the lattice; cf. [7]. For simplicity and due to the natural symmetry of the hard core, pairs of chains are attached at each of the parallelepiped corners, where each chain's first cell is the lateral extension of the respective side row of parallelepiped

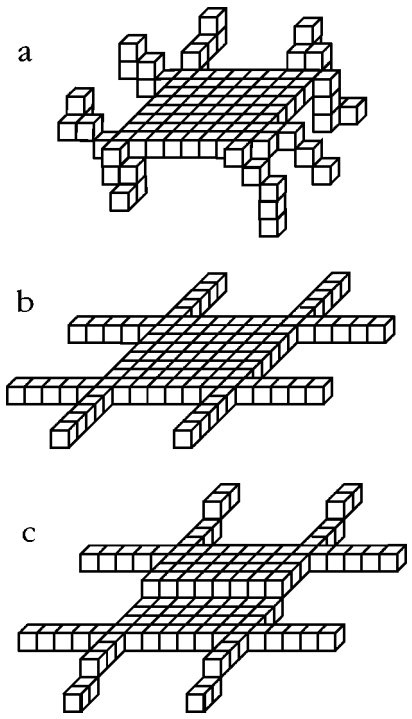

FIG. 2. Lattice representation of model discotics: an example of (a) a discotic particle with soft chains in the perfectly ordered (hard-core) nematic state, and a discotic particle with stiff chains in the state of (b) perfect order and (c) slight disorder.

cells (cf. Fig. 2), resulting in $z = 8$ chains [44]. However, for generality of presentation we allow the number of chains to be a variable as long as possible. Each of z side chains is then approximated as a Flory classical linear chain (flexible or stiff), occupying a sequence of m adjacent cells; thus the discotic molecular volume now becomes equal to $x^2 + zm$.

To retain most of the assumptions of [7], we assume that the symmetry axis of the discotic molecule is predominantly defined by the hard core, thus by the orientational order of the system we understand the order of the normal to the hard disklike core of the molecule. The declined core will be described respectively by two independent rotation angles ϕ_x and ϕ_y and the corresponding disorder indices y_X and y_Y (cf. above). Consequently, the derivation of and the final result for Z_{comb} retains a formal analogy to that of [7], which we will exploit in the following.

The model difference between the soft and stiff chain is in the orientational correlations between the subsequent lattice sites occupied by the chain, i.e., for the soft chain no such correlations are assumed, while for the stiff chain model all of the sites are orientationally correlated, i.e., a position of a subsequent site is unequivocally given by the preceding ones (cf. [1,45] and Fig. 3). The chemical potentials for the isotropic phase are approximated by setting $\overline{y_{iso}} = \overline{y_X} = \overline{y_Y} = x$ (cf. [7]).

A. Combinatoric or "steric" factor Z_{comb}

Provided j molecules are already positioned on the lattice, the number of configurations available for the $j+1$ molecule ν_{j+1} characterized by the hard-core disorder indices y_X and y_Y becomes now [cf. Eq. (3) and [7]]

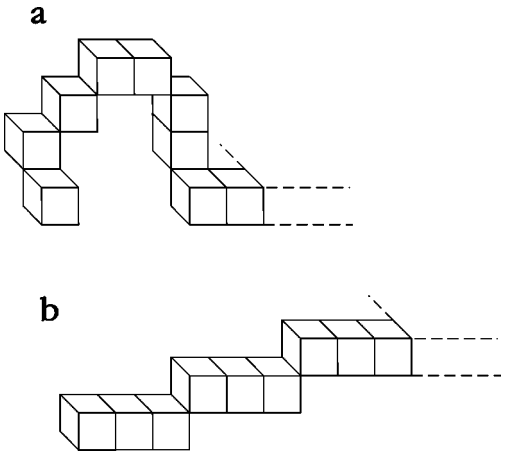

FIG. 3. Lattice representation of (a) soft and (b) stiff side chains. Broken lines indicate the position of the hard core.

$$\nu_{j+1}=n_0 P_1'^{(y_X+y_Y-1)} P_2'^{(y_X y_Y-y_X-y_Y+1)} P_c', \tag{8}$$

where $y_X y_Y$ is the number of the disk subparticles, y_X+y_Y-1 is the number of trains of subparticles the inclined disk is divided into, P_i' are the probabilities of finding free space for the ''first'' $(i=1)$ and any ''other'' $(i=2)$ segment of each train, and P_c is the probability of finding free space for the side chains. (The prime is introduced here to emphasize the presence of side chains.)

P_1' and P_2' are given by Eq. (5) with p replaced formally by p' to emphasize the presence of side chains. The probability that a given site is free for the $1a$ cell of the first segment is given by

$$p_{1a}'=\frac{n_0-j(x^2+zm)}{n_0}, \tag{9}$$

where n_0 is the total number of sites in the system (the system volume). For every other i cell p_i' is given by [cf. Eq. (12) of [7]]

$$p_i'\simeq\frac{(n_0-jx^2)}{n_0-j[(x^2+zm)-K_i(x,\overline{y};z,m)]}, \tag{10}$$

$K_i(x,\overline{y};z,m)$ being the average occupation factors that define the probabilities of finding free sites for different cells of the hard core in the presence of the chains (cf. [7] and the Appendix).

Benefiting from previous applications of the lattice method to flexible and stiff chains [36,37,46], the P_c' factor in Eq. (8), which describes the probability of additionally accommodating on the lattice z side chains, each of length m, attached to the hard core, can, to a good approximation, be written as [47]

$$P_c'=p_{1a}'^{zm\alpha}p_{2b}'^{zm(1-\alpha)} \quad \text{with} \quad 0\leqslant\alpha\leqslant 1, \tag{11}$$

where we have made use of the probabilities already defined from finding an empty site for the first cell of each sequence of collinear cells into which the chains are broken p_{1a}' and of finding a free site for each of the remaining cells in the sequence p_{2b}' [cf. Eqs. (9) and (10)], respectively; α is thus the fraction of first cells in the side chains. Note that such a definition of P_c' encompasses all encounterable kinds of side chains: from fully flexible or perfectly rigid chains to the case of chains attached to the hard core at any arbitrary angle. Such a choice also ensures model consistency in the isotropic phase and with models for rods. For example, in order to describe chains of partially relaxed stiffness it should be enough to redefine the α factor in powers in Eq. (11) in such a way that some $1a$ cells are present even in the state of perfect order (cf. above). In a similar way one can also model a solution of discotics with stiff chains, which are attached at some angle with respect to the hard-core plane. Let us consider, for example, an intuitively simple case of bowlike discotic mesogens [48,49], i.e., with the side chains bent in the same direction from the hard-core plane (cf. Fig. 4). One might intuitively expect that on average a number of $1a$ cells in chains should remain constant for small declinations of the particles from the state of perfect order. This follows from the fact that while on tilting a particle away from the perfect order the number of $1a$ cells in chains on one side of the core increases, it is simultaneously compensated for by the equal decrease of the number of $1a$ cells on the opposite side of the core [cf. Fig. 4(b)]. Such a compensation effect should be effective for declinations up to those comparable with the chain attachment angle. Since it has been observed experimentally in thermotropic discotic systems with side chains attached at an angle of about 30° that the orientational order of the discotic hard core in the nematic phase is high, e.g., $S\simeq 0.7$ at the clearing temperature [50], we expect that Eq. (11) should work for the nematic phase of bowl-like discotics quite well. In such a case α should therefore be essentially independent of $\overline{y}$ and a weak function of the core-chain bond angle. However, for simplicity and clarity of presentation we restrict our detailed considerations to two limiting cases of the side chains attached in the plane of the hard core only, as discussed below.

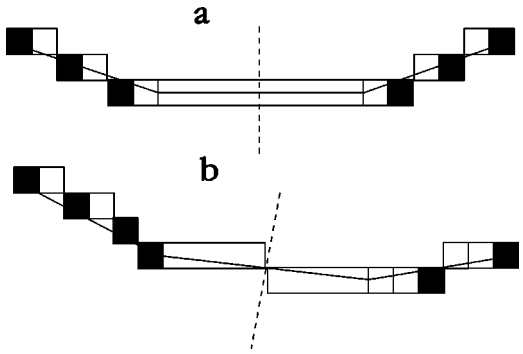

FIG. 4. Side view of a discotic particle, with side chains attached at some angle ϕ to the core plane to form a bowl-like structure in the state of (a) perfect order and (b) with some orientational disorder described by Φ. Black and white squares symbolize $1a$ and $1b$ cells, respectively.

1. Flexible chains

For soft side chains we assume, as usual, that every configuration of a chain is equally probable [36,37,45]. In terms of the lattice model the sites occupied by a given chain remain uncorrelated, i.e., every subsequent cell of the chain

can occupy a lattice site with a probability uninfluenced by the position of the preceding cell in the chain. To a good approximation we can then take the probability that a given site on the lattice is free for a given cell of a chain to be the same as for $1a$ cells of the core disk and Eq. (11) reduces to

$$P' = p_{1a}'^{zm}. \tag{12}$$

Consequently, the average occupation factors $K_i(x,\overline{y};z,m)$ for discotics with soft chains are

$$K_i^f(x,\overline{y};z,m) = K_i(x,\overline{y}) + zm, \tag{13}$$

where $K_i(x,\overline{y})$ are the ''old'' factors for a system of bare hard disks developed in [7] and the superscript f stands for ''flexible.'' The particular form of the additional term zm is a consequence of the lack of any correlations between the chains cells, i.e., every lattice site can be occupied by every cell of the soft side chain (virtual solvent). The chain cells can randomly stick out of the **XY** slice of the segment they are attached to, so given the statistical identity of all **XY** slices, they can in general block any possible site within any given slice.

With the aid of Eqs. (2) and (8)–(13), the combinatoric part of the partition function becomes

$$\begin{aligned} Z_{comb} = \frac{1}{n_x!}\prod_{j=1}^{n_x} \{ & n_0^{(1-y_X^j-y_Y^j-zm)}[n_0 - j(x^2+zm)]^{(x^2+zm)} \\ & \times F_{1b}^{-(x/y_X^j+x/y_Y^j-2)(y_X^j+y_Y^j-1)} F_{1c}^{-(y_X^j-x)(y_Y^j-x)} \\ & \times F_{2b}^{-(x/y_X^j+x/y_Y^j-2)(y_X^j-1)(y_Y^j-1)} F_{2a}^{-(y_X^j-1)(y_Y^j-1)} \}, \end{aligned} \tag{14}$$

where

$$F_i = n_0 + jM_i, \tag{15}$$

$$M_i = -(x^2+zm) + K_i^f(x,\overline{y};z,m),$$

provided $z=8$ and y_X^j and y_Y^j are the disorder indices of the j molecule. Equation (15) closely resembles the expression for Z_{comb} in [7], the only differences being the presence of the zm ''corrective'' factor. Thus the procedures of [7] can be applied in order to render Z_{comb} into a more tractable form and the steric partition function for discotic molecules with soft side chains becomes

$$\begin{aligned} -\ln Z_{comb} = {} & 2n_x(\overline{y}-1+zm/2) + n_s\ln(v_s) + n_x\ln\frac{v_x}{x^2+zm} \\ & + n_0(\overline{y}-1)^2 Q_{2a}\frac{\ln Q_{2a}}{M_{2a}} \\ & + n_0(\overline{y}-x)^2 Q_{1c}\frac{\ln Q_{1c}}{M_{1c}} \\ & + n_0(2x/\overline{y}-1)\left[(\overline{y}-1)^2 Q_{2b}\frac{\ln Q_{2b}}{M_{2b}}\right. \\ & \left. + (2\overline{y}-1)Q_{1b}\frac{\ln Q_{1b}}{M_{1b}}\right], \end{aligned} \tag{16}$$

where $Q_i = 1 + (n_x/n_0)M_i$ provided $z=8$ and M_i is defined in Eq. (15), and $v_s = n_s/n_0$ and $v_x = n_x(x^2+zm)/n_0$ are the volume concentrations of the solvent and solute, respectively.

2. Rigid, rodlike chains

We assume that each rigid chain is coplanar with the core and forms a rodlike extension of the relevant hard-core side row of cells [cf. Fig. 2(b)]. The particular position of the side chain in the molecule is of no importance for the final result due to the phase symmetry (cf. [7]).

Clearly, the ordering of stiff-chain discotics at high concentrations will be more difficult than in the case of bare disks. From simple geometric considerations of the solution in the close packing limit it becomes obvious that the solute concentration in the limit v_{VdW} rapidly decreases with m as

$$v_{VdW} = [x^2+(z-2)m][(x^2+2m)(x^2+m)]^{-1}, \tag{17}$$

i.e., from $v_{VdW}=1$ for bare hard cores to about 0.8 for $m=1$ or 0.65 for $m=2$, for illustrative values of x used in the calculations below. The concentration can increase only at the expense of orientational order of the system. Either the system will tend to a situation in which particles are perfectly orientationally and translationally inplane ordered but then, due to side chains, their centers of mass are separated substantially, at least by $x+m$, and the system density is low, or the system tends to the higher-density situation in which hard cores are as close as possible, but this would require some orientational disorder in the system to relieve steric constraints of the side chains preventing centers of mass from approaching each other more closely. These kinds of steric constraints are accommodated by our model. Once the discotic particle is tilted away from perfect order, the core disks and side chains become segmented on the lattice. Since the number and persistence of segments (their size) depend on the degree of disorder, denser packing becomes increasingly possible initially as the Flory disorder indices increase.

In order to evaluate the combinatoric part of the partition function we begin with the limiting case of perfectly ordered discotic molecules. Since in this case the side chains are the ideal extensions of the core side row cells, the side chain cells are statistically identical to the latter and (cf. Fig. 5 and the Appendix)

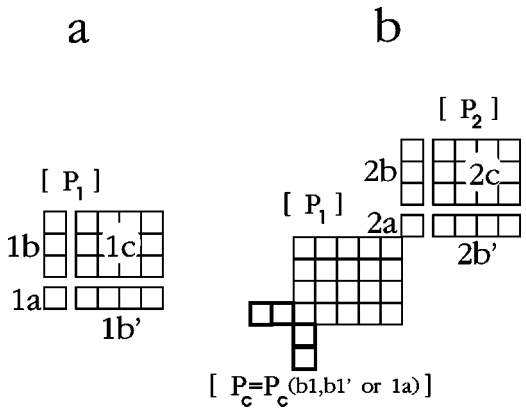

FIG. 5. Implemented segregation of (a) ''first'' $\mu=1$ and (b) ''other'' $\mu=2$ segment cells into statistically different kinds μa, μb, $\mu b'$, and μc. Cells of the side chain adjacent to the hard core are emphasized by thick lines and can be of $1b$, $1b'$, or $1a$ type; cf. the text.

$$P'=p_{2b}'^{zm}. \tag{18}$$

This leads to average occupation factors given by (cf. the Appendix)

$$\begin{aligned}
K_{1a}^{or}(x,\bar{y};z,m)&=K_{1a}^{f}(x,\bar{y};z,m),\\
K_{1b}^{or}(x,\bar{y};z,m)&=K_{1b}(x,\bar{y})+3.25m-0.25x/\bar{y}+0.25,\\
K_{1c}^{or}(x,\bar{y};z,m)&=K_{1c}(x,\bar{y})+2,\\
K_{2a}^{or}(x,\bar{y};z,m)&=K_{2a}(x,\bar{y})+4m-2x/\bar{y},\\
K_{2b}^{or}(x,\bar{y};z,m)&=K_{2b}(x,\bar{y})+2.5m-0.5x/\bar{y}+0.25,
\end{aligned} \tag{19}$$

where the superscript *or* is introduced to distinguish this particular case. In developing Eq. (19) we explicitly set $z=8$ to benefit from the system and molecule symmetry, i.e., the interchangeability of the **X** and **Y** axes. The formulas in Eq. (19) form a good quantitative approximation of the exact occupation factors as long as $0\ll m\leqslant x$; for very short side chains and for the chain length exceeding the hard-core size, the approximation is less adequate and should be used with care for qualitative extrapolation only. Fortunately, illustrative calculations show below that the orientational disorder of the nematic phase coexisting with the isotropic phase is usually relatively substantial, so the use of Eq. (19) outside the limit $0\ll m\leqslant x$ is minimized and of minor consequence for the conclusions drawn here.

The resulting combinatoric part of the partition function for the system in the state of perfect order is

$$\begin{aligned}
Z_{comb}=\frac{1}{n_x!}\prod_{j=1}^{n_x}\{&n_0^{(1-y_X^j-y_Y^j)}[n_0-j(x^2+zm)]^{(x^2+zm)}\\
&\times F_{1b}^{-(x/y_X^j+x/y_Y^j-2)(y_X^j+y_Y^j-1)}F_{1c}^{-(y_X^j-x)(y_Y^j-x)}\\
&\times F_{2b}^{-(x/y_X^j+x/y_Y^j-2)(y_X^j-1)(y_Y^j-1)-zm}F_{2a}^{-(y_X^j-1)(y_Y^j-1)}\},
\end{aligned} \tag{20}$$

where $F_i=n_0+jM_i$, and $M_i=-(x^2+zm)+K_i^{or}(x,\bar{y};z,m)$ provided $z=8$, or, applying again the usual simplifying procedure,

$$\begin{aligned}
-\ln Z_{comb}=&2n_x(\bar{y}-1)+n_s\ln(v_s)+n_x\ln\frac{v_x}{x^2+zm}\\
&+n_0(\bar{y}-1)^2Q_{2a}\frac{\ln Q_{2a}}{M_{2a}}\\
&+n_0(\bar{y}-x)^2Q_{1c}\frac{\ln Q_{1c}}{M_{1c}}\\
&+n_0(2x/\bar{y}-1)\left[(\bar{y}-1)^2Q_{2b}\frac{\ln Q_{2b}}{M_{2b}}\right.\\
&\left.+(2\bar{y}-1)Q_{1b}\frac{\ln Q_{1b}}{M_{1b}}\right]+zmQ_{2b}\frac{\ln Q_{2b}}{M_{2b}},
\end{aligned} \tag{21}$$

with the Q's and M's defined by K^{or}'s via Eqs. (16) and (20), respectively.

Now let us introduce some disorder to the system. The core disks and side chains become segmented on the lattice. Each break in the rigid chain results in generating a new segment beginning with a $1a$-type cell [1] (cf. Figs. 2 and 3). The higher the molecule declination, the more segments and $1a$ cells will be generated among zm chain cells. As a consequence of the chain stiffness and collinearity of chains with core edges, the fraction of $1a$ cells generated by disorder is proportional to the core disorder index y and is given by $\alpha=(y-1)/(x-1)$. Thus, Eq. (11) becomes

$$P_c'=p_{1a}'^{zm(y-1)/(x-1)}p_{2b}'^{zm(x-y)/(x-1)}. \tag{22}$$

For the state of perfect order $y=1$, Eq. (22) reduces to Eq. (18). In the state of complete disorder ($y=x$, the isotropic phase) the number of segments is maximum, i.e., each cell is of the $1a$ type and Eq. (22) becomes identical to Eq. (12) of the soft chains. Although the latter result might seem somewhat artificial, it is a direct consequence of the assumed statistical independence between **XY** slices. A similar problem for highly disordered rods has been discussed by Flory and other authors [2,37].

Since besides the $1a$-type cells the rest of the chain segment cells remain statistically in the state of perfect order, we assume that each occupation factor can be written as a weighted average of the appropriate K_i^f's and K_i^{or}'s

$$\begin{aligned}
K_i^r(x,\bar{y};8,m)=&\left[1-\frac{\bar{y}-1}{x-1}\right]K_i^{or}(x,\bar{y};8,m)\\
&+\left[\frac{\bar{y}-1}{x-1}\right]K_i^f(x,\bar{y};z,m).
\end{aligned} \tag{23}$$

or, with the use of Eqs.(13) and (19), explicitly

$$K^r_{1b}(x,\bar{y};z,m)=K_{1b}(x,\bar{y})+[(x-\bar{y})(3.25m+0.25x/\bar{y}+0.25)+(\bar{y}-1)zm]/(x-1),$$

$$K^r_{2b}(x,\bar{y};z,m)=K_{2b}(x,\bar{y})+[(x-\bar{y})(2.5m-0.5x/\bar{y}+0.25)+(\bar{y}-1)zm]/(x-1),$$

$$K^r_{1c}(x,\bar{y};z,m)=K_{1c}(x,\bar{y})+[(x-\bar{y})2+(\bar{y}-1)zm]/(x-1), \tag{24}$$

$$K^r_{2a}(x,\bar{y};z,m)=K_{2a}(x,\bar{y})+[(x-\bar{y})(4m-2x/\bar{y})+(\bar{y}-1)zm]/(x-1),$$

where the superscript r distinguishes the case. Since Eqs. (16) and (21) differ only in two terms, averaging over the two sets of cells is straightforward and the steric partition function for $z=8$ becomes

$$\begin{aligned}-\ln Z_{comb}=&2n_x(\bar{y}-1)+n_s\ln v_s+n_x\ln\frac{v_x}{x^2+zm}\\&+n_0(\bar{y}-1)^2Q_{2a}\frac{\ln Q_{2a}}{M_{2a}}+n_0(\bar{y}-x)^2Q_{1c}\frac{\ln Q_{1c}}{M_{1c}}\\&+n_0\frac{2x-\bar{y}}{\bar{y}}\Bigg[(\bar{y}-1)^2Q_{2b}\frac{\ln Q_{2b}}{M_{2b}}\\&+(2\bar{y}-1)Q_{1b}\frac{\ln Q_{1b}}{M_{1b}}\Bigg]+\Bigg[\frac{x-\bar{y}}{x-1}Q_{2b}\frac{\ln Q_{2b}}{M_{2b}}\\&+n_x\frac{\bar{y}-1}{x-1}\Bigg]zm,\end{aligned} \tag{25}$$

with Q's and M's defined as usual by K^r's [cf. Eqs. (16) and (20), respectively].

Equation (25) reduces to Eq. (21) in the perfect order limit, i.e., for $\bar{y}=1$. For $\bar{y}=x$ it becomes identical to Eq. (16), i.e., with the case of discotic molecules with flexible chains in the total disorder state. This result is inherent to the Flory lattice method [36,37]. Due to the **XY** ''slicing'' of the model dicotics, the soft and the strongly disordered stiff chains should be indistinguishable. However, we expect the order of the nematic phase to be relatively high, so this small inconsistency of the Flory approach should not affect our results dramatically.

B. Solute-solvent interactions Z_{int}

We examine also weak interactions between side chains and other parts of the system. For the purpose we assume that the intermolecular forces are sufficiently weak not to disturb seriously the assumed randomness for specified degree of orientation, i.e., these interactions are spatially uniform. In assuming so, we neglect the effect of the component stiffness, in particular of the side chains (c), on soft interactions in the system. The same kind of interactions have already been considered between hard disks (d) and solvent (s) in [7] and in the Flory treatment of model solutions of rodlike particles with [37] and without side chains [36].

The energy of short-range attractive interactions between the system components is usually written in the form of the van Laar heat of mixing [1,7,37]

$$\frac{\Delta E}{RT}=\chi_{sd}n_sv_d+\chi_{sc}n_sv_c+\chi_{dc}n_cv_d, \tag{26}$$

where R and T are the gas constant and temperature, respectively, and v_c and v_d are the volume concentrations of the side chains and the hard cores, respectively,

$$v_c=\frac{n_xzm}{n_0}=v_x\frac{zm/x^2}{1+zm/x^2},\quad v_d=\frac{n_xx^2}{n_0}=v_x\frac{1}{1+zm/x^2}. \tag{27}$$

$RT\chi_{ij}$ can be identified with the energy change per cell on transferring a solute molecule from the pure solute to the infinitely diluted solution.

In the case when the hard core and side chain interactions with the solvent are very similar, Eq. (26) reduces to

$$\frac{\Delta E}{RT}=\chi n_0(1-v_x)v_x+\chi_{dc}n_0\frac{zm/x^2}{(1+zm/x^2)^2}v_x^2, \tag{28}$$

with [37]

$$\chi=\chi_{sc}\frac{zm/x^2}{1+zm/x^2}+\chi_{sd}\frac{1}{1+zm/x^2}. \tag{29}$$

The contribution from interactions between side chains and hard cores χ_{dc} is, in general, nonzero. For example, it is commonly thought that the side chains in rodlike and disklike mesogens act, more of less, as a virtual solvent. One may then assume χ_{dc} to be comparable to χ_{sd} if a need arises. Note, however, that since the weighting factor $(mz/x^2)(1+zm/x^2)^{-2}$ in the last term of Eq. (28) is rather small (e.g., we found it to be less than 0.25 for a number of physically relevant numerical examples studied here), the contribution may become significant only at very high concentrations, i.e., close to the neat system, which is beyond the scope of the present paper. These interactions will then be discarded in what follows and the form of Z_{int} is the same as in [7], with χ given now by Eq. (29):

$$Z_{int}=\exp(-\Delta E/RT)=\exp(-\Theta v_xv_s). \tag{30}$$

$\Theta=\chi n_0$ may be generally thought of as a free energy of interaction [1,36,51]. On the other hand, for the convenience of results presentation of Θ is alternatively frequently interpreted as the reciprocal of the normalized (dimensionless) temperature [3,5,46,52]. Combining Eqs. (30) and (7), we get finally an expression for the Gibbs potential [cf. Eq. (33)].

C. Orientational factor Z_{or}

Since in our model the orientation of the discotic molecule remains defined by disorder indices y_X, y_Y of the hard core, Z_{or} has the same form as Eq. (30) in [7],

$$-\ln Z_{or}\simeq -2n_x\ln(\bar{y}-1). \tag{31}$$

As before, Z_{or} is related to $\bar{y}$ by the simplifying assumption that the orientational distribution function of the disk symmetry axis $f(\psi)$ is uniform over a solid angle out to some angle between the disk axis and director and zero beyond [45,7]. The presence of the side chains enters via equilibrium values of $\bar{y}$, which are strongly dependent on Z_{comb}.

D. Phase equilibria conditions

Phase equilibrium between two phases A and B requires equality of chemical potentials in both phases for all components:

$$(\mu_i-\mu_i^0)^A=(\mu_i-\mu_i^0)^B, \tag{32}$$

where $i=s$ or x denotes solvent or solute molecules, respectively. By definition, the chemical potentials are

$$\frac{\mu_i^\phi-\mu_i^0}{RT}=\left(\frac{\partial G^\phi}{\partial n_i}\right)_{T,V|eq}=-\left(\frac{\partial \ln Z^\phi}{\partial n_i}\right)_{T,V|eq}, \tag{33}$$

where $\phi\equiv A$ or B, and T and V denote the absolute temperature and sample volume, respectively. The subscript eq signifies the orientational equilibrium of solute molecules if a phase is orientationally ordered (nematic), i.e.,

$$\frac{\partial \ln Z^\phi}{\partial \bar{y}}=0, \quad \frac{\partial^2 \ln Z^\phi}{\partial \bar{y}^2}>0. \tag{34}$$

III. ILLUSTRATIVE CALCULATIONS

Results for bare disks in solution will serve as a reference. The N-I coexistence range on the dimensionless concentration-inverse temperature (v_x,Θ) phase diagrams obtained in [7] has, generally speaking, a bottlelike shape, i.e., at high temperatures it is narrow in concentration (''bottleneck'') and then, at sufficiently low temperatures, widens significantly and rapidly. For small disk axial ratios $3.015<x\leqslant 9.1$ only the coexistence of the isotropic and nematic phases is found. However, for $x\geqslant 9.1$ an additional reentrant nematic behavior just below the bottleneck shows up, i.e., in some particular range of temperatures and concentrations either of the two pairs of nematic-isotropic or nematic-nematic (N-N') phases coexist (cf. Figs. 10 and 11 in [7].

Numerical solutions of Eqs. (32) and (34) are therefore performed for two illustrative hard-core sizes representative of these two different phase behavior regimes of bare disks, i.e., for $x=7$ and 10, respectively (cf. Fig. 6). Since the number of side chains $z=8$ is fixed in the model, the phase diagram is studied as a function of stiffness and a successively increasing length of side chains. Calculations yield also the equilibrium Flory disorder index of the coexisting nematic phase $\bar{y}$. For the reader's convenience, the convention of [7] is also adopted in the figures below and $\bar{y}$ values are converted to the nematic order parameter S.

IV. RESULTS AND DISCUSSION

First, we investigate steric effects arising solely from presence of side chains, i.e., the athermal limit $\Theta=0$ (i.e., $T=\infty$). Results of calculations in the limit are summarized in Fig. 7. The critical concentration for the formation of the I-N biphase v_x^* varies nearly linearly with the chain length, increasing for the soft chains and decreasing for the stiff ones. The rate of this change increases with decreasing hard-core size [cf. Fig. 7(a)]. The shift in v_x^* is accompanied by a change in the order parameter of the coexisting nematic phase [see Fig. 7(b)]. The S dependence on the chain length is more pronounced for the larger hard core. A monotonic reduction of the nematic order by the soft chains seems to saturate on increasing the chain length. The addition of the shortest rigid chains to hard-core disks leads to a decrease of

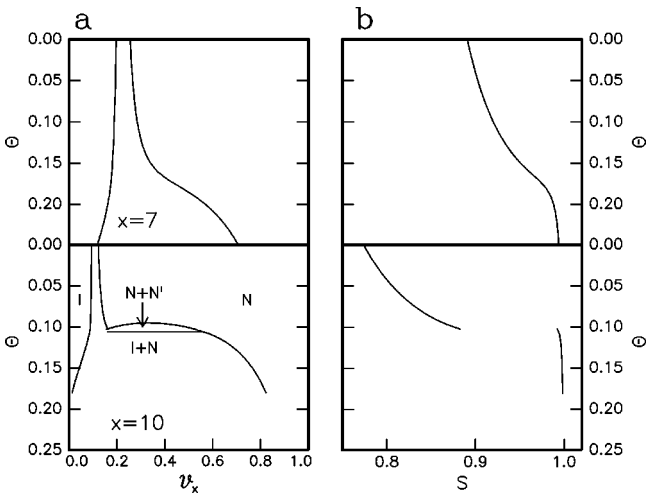

FIG. 6. (a) phase diagram (v_x,Θ) and (b) S vs Θ for two reference solutions of bare hard-core discotics of $x=7$ and 10, respectively.

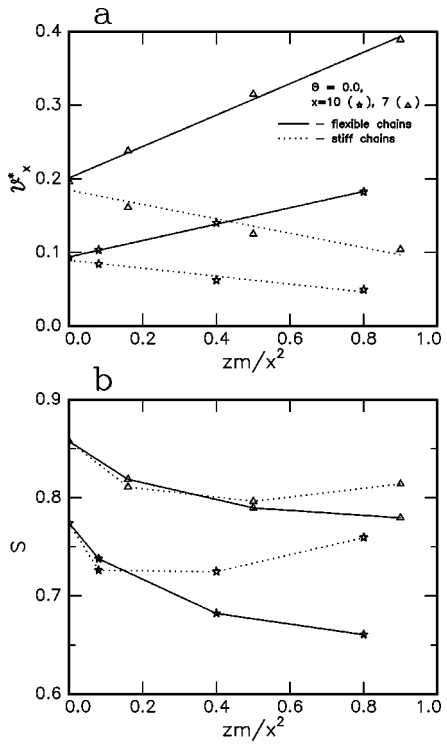

FIG. 7. Critical values of (a) v_x and (b) S for the formation of the nematic phase in the athermal limit as a function of the chain normalized volume zm/x^2. Straight lines in (a) are linear fits.

TABLE I. Critical values of parameters for the formation of the nematic phase in the athermal limit for different chain lengths.

	Soft chains	Stiff chains	
m	x_{cr}	x_{cr}	v_x^* at $x=2.05$
0	3.015	3.015	
1	4.00	2.13	
2	4.42	<1	0.604
3	4.72	<1	0.429
4	4.97	<1	0.333
5	5.18	<1	0.271
10	5.94		

the order, but on their elongation S bottoms out and begins to increase [cf. Fig. 7(b)]. The former is analogous to the decrease in the order parameter observed on increasing x in the bare disks system (cf. [7].

Some comment is necessary when comparing the results in Fig. 7 for very short chains, i.e., $m=1$. The lattice theory does not differentiate substantially between such short chains and the sole but subtle difference is how and where they are attached to the hard core (cf. Sec. II A). This leads to similar values of S, but substantially different v_x^*.

Results in Fig. 7 clearly indicate that the chain's presence influences the minimum (or critical) size of the hard core x_{cr} necessary for the formation of the nematic phase. Calculated minimum values of x for different chains are given in Table I. The inclusion of the soft chains necessitates an increase of the hard-core size and this effect seems to saturate at $x_{cr} \simeq 6$ on increasing m. Having in mind the limitations of the results in Eq. (19), we note, however, that phase diagrams for the rigid chains indicate the opposite effect. The critical hard-core size rapidly decreases below the model limit $x_{cr}=2$ on increasing m, roughly as $m+x \simeq$ const, i.e., for $m=2$ calculations give already $x_{cr}<2$. $x \simeq 1$ corresponds to yet another interesting starlike or crosslike structure of the particle. Some idea about the properties of such a system can be gained by assuming $x \simeq 2$. As an example, v_x^* vs m for $x=2.05$ and $m \geqslant 2$ are also given in Table I. The variation is dramatic. A proper study of solutions of such starlike particles requires, however, an appropriate and substantial modification of the theory, e.g., elimination of the hard core altogether and reduction of z to 4, which is beyond the scope of this paper. In addition, typical results of the phase equilibria calculations for different chains are compared with those for bare disks in Figs. 8–11.

For *soft chains* (cf. Figs. 8 and 9), independent of the hard-core size, the increasing chain length shifts the phase diagrams to higher concentrations, at the same time narrowing and extending towards lower temperatures the bottleneck section of the diagrams. The order of the nematic phase, coexisting with the isotropic phase within the bottleneck section of the phase diagram, becomes substantially suppressed and its temperature dependence weaker on increasing the chain length. However, once the biphasic range broadening is reached, S begins to rapidly rise towards unity as Θ increases further and the effect quickly saturates on increasing m (cf. Figs. 8 and 9).

Since in the case of soft chains the Gibbs free energy

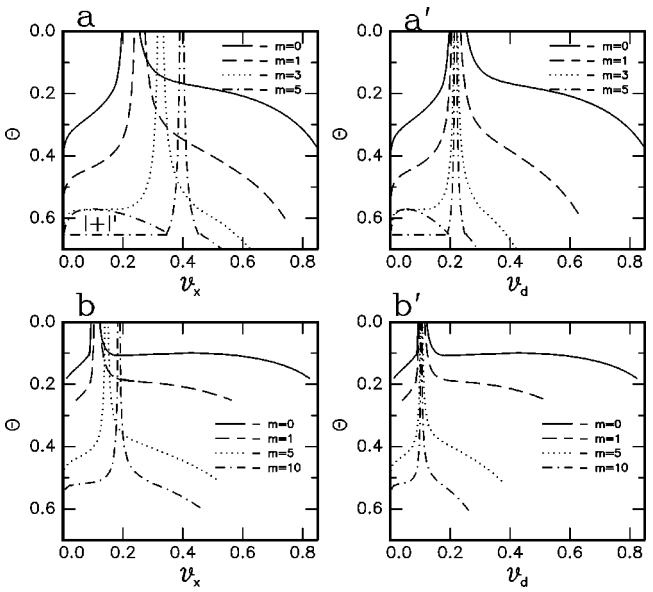

FIG. 8. Soft chain discotics: two alternative representations of the phase diagram for different hard cores (a, a') $x=7$ and (b, b') $x=10$ and different length of the side chain m. v_x and v_d are, respectively, the concentrations of discotic particles and their hard cores only.

depends only on the product of the chain number and length $zm=8m$ [cf. Eq. (16)], it is a function of neither where nor how the chains are attached to the hard core [cf. Fig. 2(a)]. The flexible chains thus play the role of an additional '''virtual'' solvent that, being isotropic, additionally separates the interacting disks cores. To demonstrate this, the phase diagram is replotted in the (v_d,Θ) coordinate system, i.e., the hard-core concentration v_d is used rather than the solvent

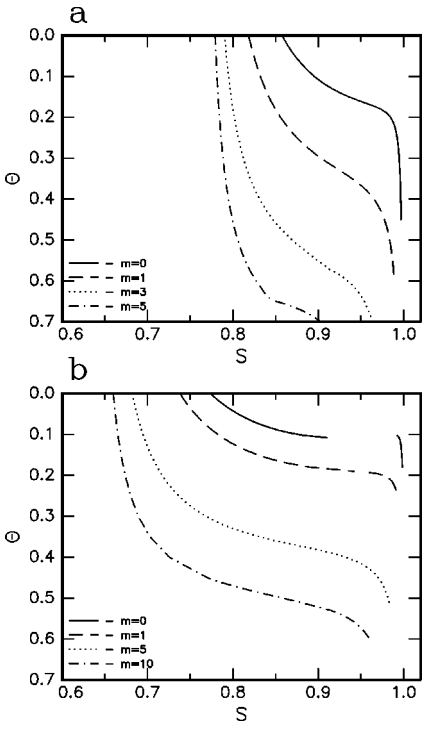

FIG. 9. Soft chain discotics: S vs Θ for the hard core of (a) $x=7$ and (b) $x=10$ and different length of the side chain m.

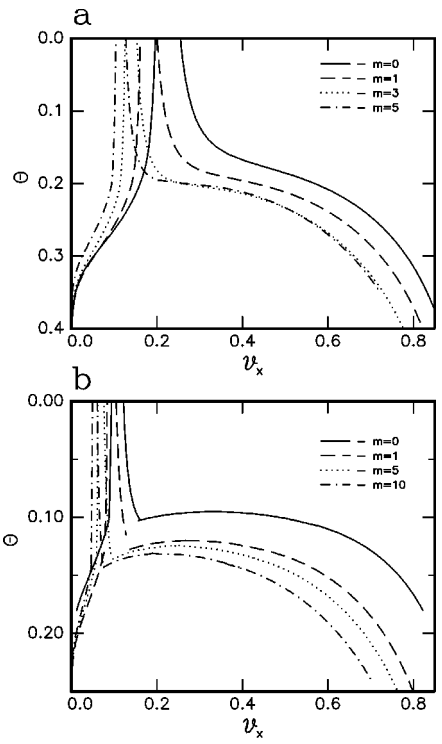

FIG. 10. Stiff chain discotics: (v_x,Θ) phase diagram for the hard core of (a) $x=7$ and (b) $x=10$ and different length of the side chain m.

concentration [cf. Eq. (27) and Figs. 8(a′) and 8(b′)]. The shift of the bottleneck towards the higher concentrations on increasing m notably disappears, but the narrowing and the offset temperature of the bottleneck range dependence on m is still pronounced. The latter can in turn be explained by the

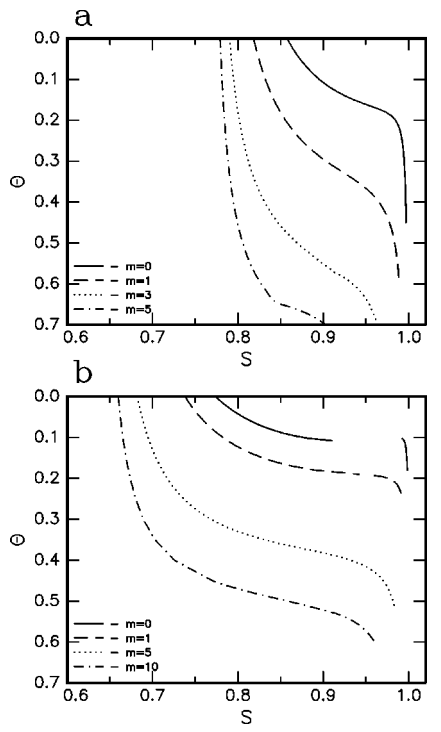

FIG. 11. Stiff chain discotics: S vs Θ for the hard core of (a) $x=7$ and (b) $x=10$ and different length of the side chain m.

absence in calculations of chain–hard-core interactions, i.e., $\chi_{dc}=0$ in Eq. (30). Trial calculations not shown here for several values of χ_{dc} indicate that inclusion of these interactions in the model indeed produces modifications of the phase diagram in the expected direction. Some of the similar disordering effects of the soft chains on a model solution of rodlike molecules were observed and discussed by Ballauff [37].

This virtual solvent effect has a consequence for the reentrant behavior observed in the system. On the one hand, calculations for $x=10$ show that the introduction of $m=1$ chains is already sufficient for the suppression of the nematic reentrant feature present for bare disks with $x\geqslant 9.1$ [cf. Figs. 8(b) and 9(b)]. In accord with numerical results in the athermal limit (cf. Table I, trial phase diagram calculations not presented here clearly indicate that the nematic reentrant phenomenon can be preserved on increasing the side chain length if the hard-core anisotropy is enlarged adequately. On the other hand, on m approaching x the phase diagram changes qualitatively in that now we have triple and critical points on the low-concentration side of the diagram, corresponding to additional coexistence region between two isotropic phases [cf. Fig. 8(b) for $m=5$]. Such a phenomenon is not unusual for discotics [53,54] and has been seen already in model lattice calculations for a solution of main-chain polymer liquid crystals [55] and mixtures of cigarlike nematogens with flexible chains [56,57]. Relative interactions become, on increasing m, strong enough to cause liquid (hard-core) -liquid (solvent) demixing in the isotropic phase [58–60].

Although soft chains act as a virtual solvent, *rigid chains* increase the discoticity of the particles, i.e., the effects of the rigid chains closely resemble those arising from increasing the axial ratio of bare disks (cf. [7]). Typical results for stiff chains are shown in Figs. 10 and 11. On increasing the chain length the *I-N* biphasic range becomes narrower and progressively shifted towards lower concentrations while the bottleneck section extends to lower temperatures. The former effect is opposite to what is observed for soft chains and reflects the enhanced discoticity of particles by the presence of stiff chains, The latter effect is analogous to that of soft chains and results from the solvent-solute interaction model adopted in the calculations, the same for both kinds of chains.

Increased discoticity results also in stabilizing the reentrant nematic behavior [cf. Fig. 10(b)]. The concentration range of the N-N' coexistence slightly decreases while the temperature range increases pronouncedly on increasing m. The enhanced discoticity is also manifested in the Θ vs S behavior. In addition to the effects associated with the initial introduction of side chains, i.e., for $m=1$, the presence of stiff chains leads to an increased order of the nematic phase. While the order parameter of the highly ordered nematic phase N' is already close to unity and thus is essentially insensitive to the presence of stiff chains, S of the less ordered nematic phase shows an isothermal increase as a function of m [cf. Fig. 11(b)].

Both principal side chain effects observed in this study, i.e., the virtual solvent effect of the soft chains and the enhanced discoticity by the stiff chains, are clearly present in thermotropic systems. Side chains in these systems are nec-

essary for both stabilizing the liquid crystallinity and providing the virtual solvent. It is very well documented in the literature that portions of aliphatic chains close to the rodlike or disklike core are rather stiff, with increasing flexibility along the chain [39,40]. This leads to a substantially larger effective hard-core part of the molecule (stabilizing effect), with the remaining flexible part of the side chain playing the role of a solvent preventing crystallization of the system.

Recent experiments with large sheetlike molecules such as palladium organyls and β-diketinate compounds confirm the importance of the side chains in their phase behavior [32]. These molecules have a flat, rigid, and more or less rectangular core and possess a large number of chains, attached to four corners in a very similar way to our model molecules. They have lyotropic properties in mixtures with apolar organic solvents. Some of the compounds also have two nematic phases in addition to the columnar one and the existence of these phases is strictly connected with the side chain's length and solvent type. The two phases differ with respect to the order parameter. The highly ordered nematic phase appears at lower temperatures and the nematic-nematic coexistence region is also observed. These properties cannot be addressed at the moment within the framework of the present theory. One should consider not only solute-solvent isotropic interactions, chain length, and stiffness, but also anisotropic interactions between the solute molecules. For rods these kind of interactions have been considered by Flory and Ronca and followers some time ago [3,5,6,61]. Our theory on the same problem in solutions of disks is well advanced [62] and on its completion we plan to return to these problems in the future.

Finally, some comment is needed on the characteristic bottleneck shape of the coexistence range on the phase diagrams. This particular shape is charactristic of many liotropic rigid mesogens with a sufficiently high shape anisotropy of molecules [63–66]. It appears to be a universal feature of such systems and is also obtainable theoretically independent of the mesogen molecular shape (disks or rods) [7,46], polydispersity [5,52,67], partial flexibility [36], the character of the intermolecular forces (orientation dependent or isotropic) [1,5,7,61,63], and the absence or presence of side chains and their stiffness [37,38] and is uninfluenced by external fields [51,68].

Note additionally that the shape of the phase diagram is asymmetric. The low-concentration boundary of the coexistence range $v_x^*(\Theta)$ is more or less linear in Θ. It is defined by the first appearance of the anisotropic phase in the system on increasing the solute volume fraction from the infinite dilution limit. The density of the isotropic phase saturates and the just formed anisotropic phase (nematic) has the lowest possible density at this point. A further increase of the solute concentration does not produce any variation of the densities (for monodisperse mesogens) until the whole system becomes nematic at the upper concentration limit of the coexistence range. Since the last bit of the isotropic phase disappears at this point, the upper concentration boundary line $v_x^{**}(\Theta)$ can be identified with the temperature dependence of the minimum (critical) density of the anisotropic phase. The latter is a function of steric and attractive intermolecular forces and varies quite dramatically on going from the regime of dominance of steric over attractive interactions to the opposite regime when the latter prevail. As a result of these dramatic changes, the phase diagram bulges on the high-concentration side. The same density changes of the nematic phase are of course also present at the low-concentration boundary. However, since the volume fraction of the anisotropic phase is then infinitely small, they show up as a slight but visible suppression of the critical volume concentration v_x^* (cf. Ref. [7] and Figs. 6, 8, and 10).

The universality of this behavior can be easily understood if one recalls the Boltzmann exponential of intermolecular energy [cf. Eq. (30)] and thinks of Θ rather as a free energy of interaction rather than the inverse of normalized temperature. In the absence of attractive interactions the density of the stable nematic solution is relatively low and requires a sufficiently large shape anisotropy of the mesogenic particles, i.e., sufficient elongation of rodlike systems [1] or flatness of disklike systems [7]. Various Flory method calculations show that if the anisotropy is below the critical value, even the maximum density of the system ($v_x=1$) is insufficient for the formation of the nematic phase in the absence of attractive forces. However, the nematic phase usually appears in such a system if attractive forces are allowed to play their role, e.g., by lowering the temperature (cf. Fig. 4 of Ref. [5] and Ref. [3]), which is characteristic of thermotropic liquid crystallinity [69,70].

For sufficient shape anisotropy, the nematic phase is formed even in the absence of attractive forces. The onset of the biphasic range occurs at ever higher solute concentrations as the shape anisotropy decreases. The transition of the whole system to a neat anisotropic state requires then a relatively small further increase of the solute concentration, i.e., the biphasic range is narrow (cf. Fig. 6). A dramatic broadening of the phase diagram signals that attractive forces are becoming important. The attractive forces bring mesogen molecules much closer to each other, thus augmenting substantially the minimum density of the stable anisotropic phase. The nematic phase is formed more easily, so the first signs of the nematic phase occur at lower concentrations. It requires, however, far more mesogenic solute molecules to sustain the continuous increase of volume fraction of the anisotropic phase in the system. Consequently, the biphasic range extends to much higher concentrations. The shape of the phase diagram for large values of Θ becomes similar to a typical demixing phase diagram of a binary system (cf., e.g., Refs. [56–58]).

Since the densities of typical mesogen compounds are very similar, one may expect that attractive forces between different parts of the system (solvent, solute, or different subsegments of the former) are of the same magnitude. Not surprisingly, the bottleneck transition feature shows up on many phase diagrams. There are, of course, some subtle differences between the phase diagrams in this region, which require separate attention. Such a study is under way and the results will be presented elsewhere.

ACKNOWLEDGMENTS

This work was supported under State Committee for Scientific Research, Poland (KBN), Grant No. 2P03B221008 and EC Human Capital and Mobility Network Project No. ERBCIPDCT 940607. Special appreciation goes to Dr. K. Earle for his many valuable suggestions.

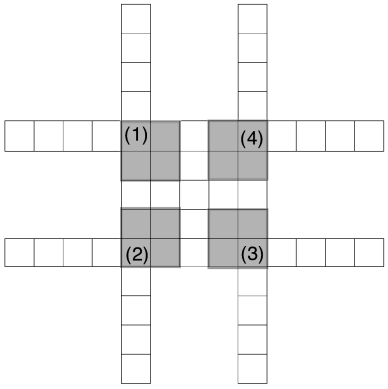

FIG. 12. Implemented labeling of hard-core corners for calculating contributions to Z_{comb} from the side chains.

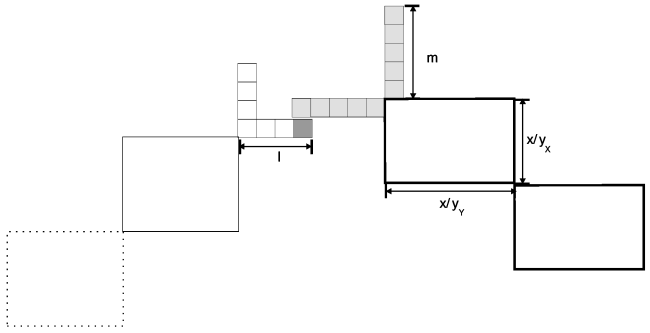

FIG. 13. Blocking ability of the terminal segment of a train with two stiff side chains of length m attached at position 1. The blocking train of type II is to the right, the placed train is to the left. Solid rectangles denote segments already positioned in the slice. l denotes the position of a chain cell with respect to corner 4. x/y_X and x/y_Y define the size of the blocking big rectangle; cf. the text.

APPENDIX

The general methodology adopted here is similar to that developed in [7] and we will when possible benefit from results derived there [7]. We consider a solution of stiff chain discotics in a state of perfect or nearly perfect order, by which we understand that the allowed disorder of the discotics is such that $x/\overline{y} \simeq x$. Furthermore, we assume that the chains are not longer than the core edge $m < x$; thus the chains' presence causes only some perturbation to the phase equilibria behavior of sole hard-core disks in solution.

Let the corner cells of the hard core the chains are attached to be labeled from 1 to 4, as shown in Fig. 12. A disordered discotic core on the lattice is segmented into connected trains of segments (cf. Fig. 4 in [7]). It follows from inspection of Fig. 2 that the side chains are at most attached to three such trains. The blocking ability of the remaining trains is the same as in the case of bare disks and the relevant occupation factors developed in [7] will be applicable also in the present case [cf. Eqs. (17)–(20) in [7]]. Thus our task reduces only to an estimate of the additional hinderance to placing cells arising from trains with side chains.

We consider the blocking ability of trains from already dissolved j discotic molecules. In the spirit of [7], it is assumed that the disorder index of all these molecules has its ensemble average value $y_X + y_Y = 2\overline{y}$. Thus each of these molecules is segmented into either type-I or type-II trains, depending on the particular orientation of a given molecule (cf. Fig. 4 in [7]). Due to the system symmetry, both types of trains should be equally probable. As we argued in [7], the final result for a given occupation factor is the arithmetic mean of results for both types of trains. Since the system should be in equilibrium, we assume that the disorder index of $j+1$ molecule is also close to the system mean value $\overline{y}$. Without limiting the generality of considerations, we assume that the considered $j+1$ discotic is represented on the lattice by the type-I trains (cf. [7]). Each particular site is discussed in the following.

1. Factor K_{1a}

A site for the $1a$ cell can be occupied by any cell of the chains, consistent with the result for soft side chains [cf. Eq. (13)].

2. Factor K_{2a}^{or}

A site for the $2a$ cell can already be occupied by trains with the side chains in several different ways and the number of ways side chains can do this is summarized in Table II.

It follows from Table II that the sole difference between type-I and type-II blocking trains is in the blocking ability of chains attached at position 4, i.e., since $m \leqslant x$ and $x/\overline{y} \approx x$, for the type-II trains access of the chains to the $2a$ site is blocked by the segment they are attached to.

Combining the results in Table II and contributions from the $2\overline{y} - 1 - 3$ chainless trains, one gets the occupational factor of the $2a$ site by type-I blocking trains,

$$N_{2a}^{I} = (2\overline{y} - 2)(2x/\overline{y} - 1) + 4m - 1 = (2\overline{y} - 1)(2x/\overline{y} - 1) + 4m - 2x/\overline{y}, \tag{A1}$$

and by type-II trains,

$$N_{2a}^{II} = (\overline{y^2} - 1)(2x/\overline{y} - 1) + 4m - 1 = (\overline{y^2})(2x/\overline{y} - 1) + 4m - 2x/\overline{y}. \tag{A2}$$

The arithmetic average of results in Eqs. (A1) and (A2) yields

TABLE II. Number of ways trains with side chains can block a site for the $2a$ cell.

Side chains attached at position (cf. Fig. 12)				Type of
1	2	3	4	blocking train
$2x/\overline{y} + m - 2$	$2m + 1$	$2x/\overline{y} + m - 2$	$2m + 1$	I
$2x/\overline{y} + m - 2$	$2m + 1$	$2x/\overline{y} + m - 2$	0	II

TABLE III. Number of ways type-II trains with side chains can block the $1b$ site.

	$m-l<0$		$m-l\geq 0$	
Chains	Small	Big	Small	Big
1		$x/\overline{y}+m$	$m+1$	$m+(x/\overline{y}-l)$
2		$x/\overline{y}+m$	$(m-l)+x/\overline{y}$	
3	$x/\overline{y}+m$	0	$x/\overline{y}+m$	$m-l$
4		$x/\overline{y}+m$	$x/\overline{y}+m$	
N	$x\overline{y}+4m$	$(2\overline{y}-1)x/\overline{y}+3m$	$x\overline{y}-x/\overline{y}+4m-l+1$	$(2\overline{y}-1)x/\overline{y}+4m-3l$

$$K_{2a}^{or}(x,\overline{y},z,m)=\frac{1}{2}(N_{2a}^{I}+N_{2a}^{II})=\frac{1}{2}(2x/\overline{y}-1)(\overline{y^2}+2\overline{y}-1)+4m-2x/\overline{y}. \tag{A3}$$

3. Factor K_{1b}^{or}

The side row $1b$ and $1b'$ cells are placed interchangeably (cf. [7]) Let us now consider a site within a distance l from the segment's $1a$ corner. For type-II blocking trains we need to consider four separate cases due to different relations between l and the chain length ($m-l<0$ or $m-l\geq 0$) and the segment size ($x/y_Y>l$ or $x/y_Y<l$) see (Fig. 13). Note that under the assumption $y_X+y_Y=2\overline{y}$, if $x/y_Y>l$ then $x/y_X<l$ and the vice versa. The segments with $x/y_Y>l$ are further referred to as ''big,'' and those with $x/y_Y<l$ as ''small.'' An example of a big blocking segment is shown in Fig. 13. Occupancies for chains attached at different positions and the occupation factors N arising from type-II blocking trains (chainless included) for the each case are summarized in Table III.

Note that for $m-l<0$ occupancies are l independent, as one should expect. We average occupancies for $m-l\geq 0$ and l from 0 to m by setting $l=m/2$. Next, we arithmetically average over the rectangle size, i.e., we take the average of the N in small and big columns in Table III. For $m-l<0$ we get from Table III

$$N_{m<l}=[1/2\overline{y^2}+1/2(2\overline{y}-1)]x/\overline{y}+3.5m \tag{A4}$$

and for $m-l\geq 0$

$$N_{m\geq l}=[1/2\overline{y^2}+1/2(2\overline{y}-1)]x/\overline{y}+3m-1/2(x/\overline{y}-1). \tag{A5}$$

Since results in Eqs. (A4) and (A5) do not differ significantly, we expect that the occupation factor for $1b$ sites K_{1b}^{or} should be approximated with a satisfactory accuracy by the arithmetic mean of the two:

$$N_{1b}^{II}=\frac{1}{2}(N_{m<l}+N_{m\geq l})=1/2(\overline{y^2}+2\overline{y}-1)(x/\overline{y})+3.25m-0.25x/\overline{y}+0.25. \tag{A6}$$

In the case of type-I blocking trains, corrections introduced by the presence of chains are similar to those of type-II trains, except for chains attached at corner 3 (cf. Table IV). Again, contributions from the remaining chainless segments are appropriately taken care of in the respective N factors.

Occupancies are averaged first for $m-l\geq 0$ over l from 0 to m by again setting $l=m/2$ and next we arithmetically average over the rectangle sizes. For $m-l<0$ we obtain

$$N_{m<l}=x\overline{y}+3.5m \tag{A7}$$

and for $m\geq l$

$$N_{m\geq l}=x\overline{y}-0.5x/\overline{y}+3m+0.5 \tag{A8}$$

(cf. Table IV). Thus, the final contribution to the occupation factor from the ''average'' molecule built of type-I trains is

$$N_{1b}^{I}=\frac{1}{2}(N_{m<l}^{I}+N_{m\geq l}^{I})=x\overline{y}-0.25x/\overline{y}+0.25+3.25m \tag{A9}$$

and using Eq. (A6) one finally gets

$$K_{1b}''(x,\overline{y},8,m)=\frac{1}{2}(N_{1b}^{I}+N_{1b}^{II})=[3\overline{y^2}/4+(2\overline{y}-1)/4]x/\overline{y}+3.25m-0.25x/\overline{y}+0.25 \tag{A10}$$

4. Factor K_{2b}^{or}

Since for type-II trains the blocking ability of their subsequent segments is independent of the presence of the preceding segments in the train being placed, the contribution from type-II trains to the occupancy of the $2b$ site will be the same as for the $1b$ sites [cf. the case of bare disks, Eq. (A15) in [7]]. Thus, we need to estimate in this case the contributions from type-I trains only.

TABLE IV. Number of ways type-I trains with side chains can block the $1b$ site.

	$m-l<0$		$m-l\geq 0$	
Chains	Small	Big	Small	Big
1	$x/\overline{y}+m$		$m+1$	$m+(x/\overline{y}-l)$
2	$x/\overline{y}+m$		$(m-l)+x/\overline{y}$	
3	$x/\overline{y}+m$	$x/\overline{y}$	$x/\overline{y}+m$	$x/\overline{y}+m-l$
4	$x/\overline{y}+m$		$x/\overline{y}+m$	
N	$x\overline{y}+4m$	$x\overline{y}+3m$	$x\overline{y}-x/\overline{y}+4m-l+1$	$x\overline{y}+4m-3l$

TABLE V. Number of ways type-I trains with side chains can block the $2b$ site.

	Side chains attached at position (cf. Fig. 12)					
	1		2	3		4
Case	Small	Big	Both	Small	Big	Both
$m-l<0$	$x/\overline{y}+m$		$x/\overline{y}+m$	$x/\overline{y}+m$	$x/\overline{y}$	0
$m-l\geqslant 0$	$x/\overline{y}-l$	1	$m-l$	$x/\overline{y}+m$	$x/\overline{y}+m-l$	0

The presence in the **XY** slice of the just placed preceding segment creates severe restrictions on the blocking ability of the type-I train, i.e., access to any considered site for the $2b$ cell by cells of any other segment but the first one in the blocking train is forbidden. In particular, there will not be any contribution from chains attached to corner 4 since it belongs to the last segment in the train. The number of ways type-I trains can block a given site for the the 2b cell will again depend on the relative magnitude of l with respect to m and on the size of the blocking segment (either big or small). Following the procedure of Sec. III, we get results summarized in Table V.

Repeating the same procedure as in the previous subsections, i.e., by adding up relevant contributions and averaging over the segment size and over l, $l<m$, we get

$$N_{2b}^{I}=(\overline{y}-1)x/\overline{y}-0.75x/\overline{y}+1.75m+0.25. \quad \text{(A11)}$$

Since $N_{1b}^{II}\equiv N_{1b}^{I}$, with the aid of Eq. (A6) the occupation factor becomes

$$K_{2b}^{or}(x,\overline{y},8,m)=\frac{1}{2}(N_{2b}^{I}+N_{1b}^{II})=[\overline{y^2}/4+3(2\overline{y}-1)/4]x/\overline{y} - 0.5x/\overline{y}+2.5m+0.25. \quad \text{(A12)}$$

5. Factor K_{1c}^{or}

Blocking of sites destined for μc cells, $\mu=1$ or 2, strongly depends on how the considered cell position in the segment compares with the obstructing chain length. The sites for more ''outer'' μc cells can be blocked even by very short chains, whereas the inner ones can only be blocked by the longer. We note also that chains attached at corner 4 of any of the potentially obstructing trains do not participate in the blocking. One thus needs to consider only chains attached to the remaining three corners. Furthermore, contributions from the chains are the same regardless of the train type, i.e., I or II, the chains are attached to. The mean occupation factor for μc cells K_{1c}^{or} can be written generally as

$$K_{1c}^{or}(x,\overline{y},z,m)=\tfrac{1}{2}[(\overline{y^2}-3)+2\overline{y}-4]+h, \quad h=\sum_{i=1}^{3} p_{(i)}, \quad \text{(A13)}$$

where the blocking contributions $p_{(i)}$ from chains attached to the ith corner are *explicitly* separated. As trial calculations show, the phase diagram turns out to be very sensitive to the value the h parameter takes on. Nevertheless, in order to simplify the final formulas and to facilitate drawing some conclusions from numerical results of the present work, we decided to find some reasonable approximate mean value of the parameter, which would allow the main features of the system behavior on varying m to be preserved. Note, for example, that the value of h increases from 2, characteristic for the innermost cells, to 6 for the outermost cells. Since the number of equivalent cells (and thus the statistical weight) increases with the distance from the μa cell, one should expect the average value of h to be greater than the arithmetic mean of both extrema, i.e., 4. To get a more realistic approximation of the mean we consider the segment middle cell, i.e., the one at a position $[x/2\overline{y},x/2\overline{y}]$ with respect to μa corner (cf. Fig. 5). Particular values of $p_{(i)}$ depend on whether $m<x/2\overline{y}$ or $m>x/2\overline{y}$. For $m<x/2\overline{y}$ we have

$$p_{(1)}=1, \quad p_{(2)}=2, \quad p_{(3)}=1 \quad \text{(A14)}$$

and for $m>x/2\overline{y}$

$$p_{(1)}=2, \quad p_{(2)}=2, \quad p_{(3)}=2. \quad \text{(A15)}$$

The average of h from Eqs. (A14) and (A15) is 5. The value enhances the contribution from very short chains $x \gg 2 \geqslant m$ in particular, but should work better for chains with m approaching x. Nevertheless, we decided to use it in our illustrative calculations. This leads obviously to some uncertainty in the phase diagram behavior on m approaching 0, as illustrated in Fig. 14. Note that the phase diagram is essentially insensitive to h in the bottleneck part of the biphasic range. The main effect of h is then a shift of the broad part of the phase diagram towards lower temperatures on increasing h from 5 to 6. The effect becomes quickly less pronounced on increasing m, thus the approximation gives more realistic results for longer chains. Of course, if the need arises, a value of h for any particular fixed chain length can be precisely estimated and used in Eq. (A13). Substitution of the mean value $h=5$ into Eq. (A13) gives

$$K_{1c}^{or}(x,\overline{y},z,m)=\tfrac{1}{2}[(\overline{y^2}-3)+2\overline{y}-4]+5. \quad \text{(A16)}$$

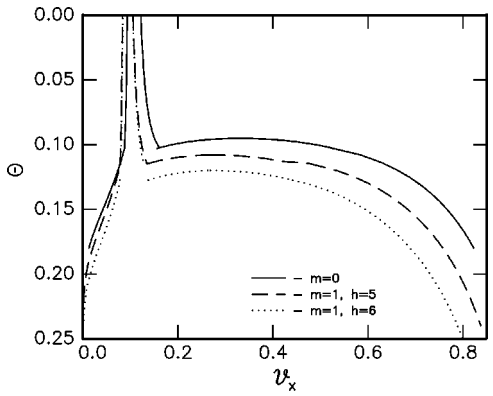

FIG. 14. Effect of the h correction factor appearing in Eq. (A13) on the (v_x,Θ) phase diagram for $x=10$. The phase diagram for the pure hard-core system of $x=10$ is also shown; cf. the text.

[1] P. J. Flory, Proc. R. Soc. London, Ser. A **234**, 73 (1956).
[2] P. J. Flory and G. Ronca, Mol. Cryst. Liq. Cryst. **54**, 289 (1979).
[3] P. J. Flory and G. Ronca, Mol. Cryst. Liq. Cryst. **54**, 311 (1979).
[4] M. A. Cotter and D. E. Martire, J. Chem. Phys. **53**, 4500 (1970).
[5] M. Warner and P. J. Flory, J. Chem. Phys. **73**, 6327 (1980).
[6] J. K. Moscicki, J. Polym. Sci., Polym. Phys. Ed. **23**, 327 (1985).
[7] M. Wnek and J. K. Moscicki, Phys. Rev. E **53**, 1666 (1996).
[8] L. Onsager, Ann. (N.Y.) Acad. Sci. **59**, 627 (1949).
[9] A. Stroobants and H. N. W. Lekkerkerker, J. Phys. Chem. **88**, 3669 (1984).
[10] S. Chandrasekhar, B. Sadashiva, and K. Sureah, Pramana **9**, 471 (1977).
[11] N. Huu Tinh, C. Destrade, and H. Gasparoux, Phys. Lett. **72A**, 251 (1979).
[12] S. Chandrasekhar and G. S. Ranganath, Rep. Prog. Phys. **53**, 57 (1990).
[13] N. Boden, J. Clements, K. A. Dawson, K. W. Jolley, and D. Parker, Phys. Rev. Lett. **66**, 2883 (1991).
[14] T. K. Attwood, Y. E. Lydon, and F. Jones, Liq. Cryst. **1**, 499 (1986).
[15] N. Boden, R. J. Bushby, L. Ferris, C. Hardy, and F. Sixl, Liq. Cryst. **1**, 109 (1986).
[16] K. Praefcke, D. Singer, and B. Gundogan, Mol. Cryst. Liq. Cryst. Sci. Technol., Sect. A **223**, 181 (1992).
[17] N. Usoltsewa, K. Praefcke, D. Singer, and B. Gundogan, Liq. Cryst. **16**, 601 (1994).
[18] Z. Belarbi, M. Maitrot, K. Ohta, J. Simon, J. J. Andre, and P. Petit, Chem. Phys. Lett. **143**, 400 (1988).
[19] J. F. Van der Pol, E. Neelemen, J. W. Zwikker, R. J. Nolte, W. Drenth, J. Aerts, R. Visser, and S. J. Picken, Liq. Cryst. **6**, 577 (1989).
[20] Y. Hendrikx, J. Charvolin, M. Rawiso, L. Liebert, and M. C. Holmes, J. Phys. Chem. **87**, 3992 (1983).
[21] Y. Galerne, A. M. Figueiredo Neto, and L. Liebert, Phys. Rev. A **31**, 4047 (1985).
[22] C. Rosenblatt, J. Phys. (Paris) **47**, 1097 (1986).
[23] D. Frenkel and B. M. Mulder, Mol. Phys. **55**, 1171 (1985).
[24] S. Chandrasekhar, Liq. Cryst. **14**, 3 (1993).
[25] C. Destrade, M.C. Mondon-Bernaud, and N. H. Tinh, Mol. Cryst. Liq. Cryst. **49**, 169 (1979).
[26] N.H. Tinh, H. Gasparoux, and C. Destrade, Mol. Cryst. Liq. Cryst. **63**, 1049 (1981).
[27] M. Sorai and H. Suga, Mol. Cryst. Liq. Cryst. **73**, 47 (1981),
[28] J. Lejay and M. Pesquer, Mol. Cryst. Liq. Cryst. **95**, 31 (1983).
[29] S. Takenaka, K. Nishimura, and S. Kusabayashi, Mol. Cryst. Liq. Cryst. **111**, 227 (1984).
[30] M. ReyLafon, C. Destrade, and A.T. Hemida, Mol. Cryst. Liq. Cryst. **137**, 381 (1986).
[31] K. Praefcke, B. Biligin, N. Usoltsewa, B. Heinrich, and D. Guillon, J. Mater. Chem. **5**, 2257 (1995).
[32] N. Usoltsewa, G. Hauck, H. D. Koswig, K. Praefcke, and B. Heinrich Liq. Cryst. (to be published).
[33] K. Praefcke (private communication).
[34] D. Frenkel, J. Chem. Phys. **91**, 4912 (1987).
[35] J.G. Gay and B.J. Berne, J. Chem. Phys. **74**, 3316 (1981).
[36] R. R. Matheson and P. J. Flory, Macromolecules **14**, 954 (1981).
[37] M. Ballauff, Macromolecules **19**, 1366 (1986).
[38] M. Ballauff, Liq. Cryst. **2**, 519 (1987).
[39] N. Boden, S. A. Jones, and F. Sixl, Biochemistry **30**, 2146 (1991).
[40] R.Y. Dong, *Nuclear Magnetic Resonance in Liquid Crystals* (Springer-Verlag, New York, 1994).
[41] K. A. Dill and Paul J. Flory, Proc. Natl. Acad. Sci. USA **77**, 3115 (1980).
[42] K. A. Dill and Paul J. Flory, Proc. Natl. Acad. Sci. USA **78**, 676 (1981).
[43] K. A. Dill, D. E. Koppel, R. S. Cantor, J. D. Dill, D. Bendedouch, and S.-H. Chen, Nature (London) **309**, 42 (1984).
[44] $z=8$ is a reasonable choice for sufficiently large hard cores. For small hard cores the side chains become too overcrowded to be good model for a real system; cf. Fig. 2. Lowering the number of chains to, e.g., $z=4$ and thus enabling modeling of starlike or crosslike particle solutions is possible; however, it would significantly and unnecessarily increase the complexity of the theory and is beyond the scope of the present paper.
[45] P. J. Flory, Proc. R. Soc. London, Ser. A **234**, 60 (1956).
[46] P. J. Flory, Adv. Polym. Sci. **59**, 1 (1984).
[47] Equation (11)) is not an exact expression for P_s. Since the subsequent segments of the side chain are no longer in the **XY** slice of the subparticle train the chain is attached to, the conditional probabilities of finding vacancies for them is more appropriately expressed by p_{1b} (cf. Fig. 12). However, the difference between the p_{1b} and p_{2b} is negligibly small within the lattice method accuracy to justify the use of p_{2b}. In return, we avoid introducing additional disorder parameters for the chains.
[48] K. M. Leung and Lin Lei, Mol. Cryst. Liq. Cryst. **146**, 71 (1987).
[49] L.-Y. Wang, Z.-M. Sun, X.-F. Pei, and Y.-P. Zhu, Chem. Phys. **142**, 335 (1990).
[50] See, for example, S. Zamir, D. Singer, N. Spielberg, E.J. Wachtel, H. Zimmermann, R. Poupko, and Z. Luz, Liq. Cryst. **21**, 39 (1996).
[51] Y. Aikawa, N. Minami, and M. Sukigara, Mol. Cryst. Liq. Cryst. **70**, 115 (1981).
[52] J. K. Moscicki and G. Williams, Polymer **23**, 558 (1982).
[53] T. Warmerdam, D. Frenkel, and R. J. J. Zijstra, Liq. Cryst. **3**, 149 (1988).
[54] T. W. Warmerdam, R. J. Nolte, W. Drenth, J. C. van Miltenburg, D. Frenkel, and R. J. J. Zijstra, Liq. Cryst. **3**, 1087 (1988).
[55] A. P. Khokhlov and A. N. Semenov, J. Stat. Phys. **38**, 161 (1985).
[56] M. Ballauff, Mol. Cryst. Liq.. Cryst., Lett. Sect. **4**, 15 (1986).
[57] H. Orendi and M. Ballauff, Liq. Cryst. **6**, 497 (1989).
[58] G. Sigaud, H. T. Nguyen, M. F. Achard, and R. J. Twieg, Phys. Rev. Lett. **65**, 2796 (1990).
[59] P. Bolhuis, *Liquid-like Behavior in Solids, Solid-like Behavior in Liquids* (FOM, Amsterdam, 1996).
[60] F. C. Frank and A. Keller, Polym. Commun. **29**, 186 (1988).
[61] C. Counsell and M. Warner, Mol. Cryst. Liq. Cryst. **83**, 307 (1983).
[62] D. Sokolowska and J. K. Moscicki (private communication).
[63] J. K. Moscicki, Adv. Chem. Phys. **63**, 631 (1985), and references therein.
[64] W. G. Miller, L. Kou, K. Tohyama, and V. Voltaggio, J. Polym. Sci., Polym. Symp. **65**, 91 (1978).

[65] V. G. Kulichikhin, G. I. Kudryavtsev, and S. P. Papkov, Int. J. Polym. Mater. **9**, 239 (1982).
[66] S. M. Aharoni, J. Polym. Sci., Polym. Phys. Ed. **18**, 1439 (1980).
[67] J. P. Flory and A. Abe, Macromolecules **11**, 1119 (1978).
[68] M. Wnek and J. K. Moscicki (unpublished).
[69] P. G. de Gennes, *Physics of Liquid Crystals* (Clarendon, Oxford, 1974).
[70] G. Vertogen and W. H. de Jeu, *Thermotropic Liquid Crystals, Fundamentals* (Springer, New York, 1988).